Carbohydrate Polymers 90 (2012) 1757–1763

Contents lists available at SciVerse ScienceDirect

Carbohydrate Polymers

journal homepage: www.elsevier.com/locate/carbpol

Nanocrystalline cellulose (NCC) reinforced alginate based biodegradable nanocomposite film

Tanzina Huq[a], Stephane Salmieri[a], Avik Khan[a], Ruhul A. Khan[a], Canh Le Tien[a], Bernard Riedl[b], Carole Fraschini[c], Jean Bouchard[c], Jorge Uribe-Calderon[d], Musa R. Kamal[d], Monique Lacroix[a,*]

[a] Research Laboratories in Sciences Applied to Food, Canadian Irradiation Centre (CIC), INRS-Institut Armand-Frappier, University of Quebec, 531 Boulevard des Prairies, Laval, Québec, H7V 1B7, Canada
[b] Département des sciences du bois et de la forêt, Faculté de foresterie, géographie et géomatique, Université Laval, Québec, G1V 0A6, Canada
[c] FPInnovations, 570 Boulevard St. Jean, Pointe-Claire, Québec, H9R 3J9, Canada
[d] Department of Chemical Engineering, McGill University, 3610 University Street, Montreal, QC H3A 2B2, Canada

ARTICLE INFO

Article history:
Received 27 April 2012
Received in revised form 12 July 2012
Accepted 26 July 2012
Available online 1 August 2012

Keywords:
Alginate
Nanocrystalline cellulose
Nanocomposite
Biopolymers
Morphology
Thermal properties

ABSTRACT

Nanocrystalline cellulose (NCC) reinforced alginate-based nanocomposite film was prepared by solution casting. The NCC content in the matrix was varied from 1 to 8% ((w/w) % dry matrix). It was found that the nanocomposite reinforced with 5 wt% NCC content exhibits the highest tensile strength which was increased by 37% compared to the control. Incorporation of NCC also significantly improved water vapor permeability (WVP) of the nanocomposite showing a 31% decrease due to 5 wt% NCC loading. Molecular interactions between alginate and NCC were supported by Fourier Transform Infrared Spectroscopy. The X-ray diffraction studies also confirmed the appearance of crystalline peaks due to the presence of NCC inside the films. Thermal stability of alginate-based nanocomposite films was improved after incorporation of NCC.

1. Introduction

Recent years there have been remarkable developments in the polymeric packaging films for improving the preservation of packaged foods. These films possess the potential for improving stability of foods by acting on the food surface, upon contact (Cha, Choi, Chinnan, & Park, 2002). Biodegradable polymers known for many decades, these polymers have been ignored mainly because of the low cost of synthetic polymers. However the biodegradable polymers could replace synthetic polymers in many applications, thus reducing the problems of disposability of traditional plastics. In an effort to produce more environment-friendly materials, renewable and biodegradable polymers have been investigated in different fields. Biopolymer films which contain polysaccharide ingredients enable us to obtain edible films with good mechanical and water barrier properties (Briassoulis, 2006).

Alginate is the most widely used material for biopolymeric film. It is a natural polysaccharide derived from marine plants and its basic structure consists of linear unbranched polymers containing β-(1→4)-linked D-mannuronic acid (M) and α-(1→4)-linked L-guluronic acid (G) residues (Khan et al., 2010, Khan, Huq, Saha, Khan, & Khan, 2010). The chemical composition and sequence of the M and G residues depend on the biological source and the state of maturation of the plant. The stiffness of the three blocks decreases in the order GG > MM > MG. Alginate forms a thermally stable and biocompatible hydrogel in the presence of di- or tri-cations. Alginate is of interest as a potential biopolymer film component because of its unique colloidal properties, which include thickening, stabilizing, suspending, film forming, gel producing, and emulsion stabilizing (Draget, Braek, & Smidsrod, 1994; Fabra, Talens, & Chiralt, 2008; Han, Guenier, Salmieri, & Lacroix, 2008; Salmieri & Lacroix, 2006).

Cellulose is a fascinating biopolymer, subject of intensive research and development and a sustainable raw material. Cellulose has gained interest as a renewable, environmentally friendly, and cost-effective reinforcing agent for composite materials (Samir, Alloin, & Dufresne, 2005). Cellulose is a natural homopolymer composed of D-glucopyranose units which are linked together by β-(1→4)-glycosidic bonds (Klemm, Schumann, Kramer, Koth, & Sultanova, 2009). Nanocrystalline cellulose (NCC) is composed of rod-like shaped nanoparticles, and it can be referred to nanocrystals, whiskers or nanowhiskers. NCC can be prepared from wood pulp by controlled acid hydrolysis. The use of sulfuric acid imparts negative charges to the NCC, thus preventing the NCC particles to

* Corresponding author. Tel.: +1 450 687 5010; fax: +1 450 686 5501.
E-mail address: monique.lacroix@iaf.inrs.ca (M. Lacroix).

0144-8617/$ – see front matter © 2012 Elsevier Ltd. All rights reserved.
http://dx.doi.org/10.1016/j.carbpol.2012.07.065

aggregate. The NCC suspension is very stable over time. These cellulose nanocrystals are featured by an average diameter of 5–10 nm and an average length of around 100 nm. NCC exhibits very interesting properties such as renewable nature, low density, high specific strength and modulus, large and highly reactive surface which can be used for grafting specific groups. Thus, NCC is very interesting nanomaterial for production of low-cost, lightweight, and very strong nanocomposites (Beck-Candanedo, Roman, & Gray, 2005; Habibi, Lucia, & Rojas, 2010).

The main objective of this work was to develop a renewable and biodegradable alginate based nanocomposite films by incorporating NCC for food-packaging applications. The effect of NCC loading on the mechanical, barrier and thermal properties of the alginate matrix was evaluated.

2. Materials and methods

2.1. Materials

Sodium alginate (alginic acid sodium salt from brown algae, guluronic acid content ~65–70%; mannuronic acid content ~5–35%) and calcium chloride (granules) were purchased from Sigma–Aldrich Canada Ltd. (Oakville, ON, Canada). Nanocrystalline cellulose (NCC) was produced in FPInnovations pilot plant reactor (Pointe-Claire, QC, Canada) from a commercial bleached softwood kraft pulp according to a procedure modified from the literature (Dong, Revol, & Gray, 1998).

2.1.1. Preparation of alginate based films

An aqueous solution containing 3% alginate (w/v) and 1–8% (w/w) NCC in dry wt relative to that of dry matrix was homogenized using a Ultra-Turrax TP18/1059 homogenizer (Janke & Kunkel, Staufen, Germany) at 23 °C and 25,000 rpm for 1 min (Salmieri & Lacroix, 2006). Films were cast by pouring 10 mL of the film forming solution into Petri dishes and allowed to dry for 24 h, at room temperature and 35% relative humidity (RH). Then the films were treated with 1% $CaCl_2$ solution and washed several times with distilled water to remove the excess $CaCl_2$ present in the films. The films were again dried as described above under the same condition for 6–8 h and the dried water insoluble films were peeled off manually using a spatula and stored in polyethylene bags prior to characterization.

2.2. Mechanical properties measurement

2.2.1. Film thickness

Thickness of the films (25–35 μm) was measured using a Mitutoyo digimatic Indicator (Type ID-110E; Mitutoyo Manufacturing Co. Ltd, Tokyo, Japan) with a resolution of 1 μm, at five random positions around the film, by slowly reducing the micrometer gap until the first indication of contact.

2.2.2. Tensile strength, tensile modulus and elongation at break

The films were equilibrated in a desiccator containing a saturated sodium bromide solution ensuring 56% RH at room temperature (21 °C) for at least 24 h. Tensile strength (TS), tensile modulus (TM) and elongation at break (Eb%) of the films were measured with a Universal Tensile Machine (Model H5KT, Tinius-Olsen Inc., Horsham, PA, USA,) equipped with a 100 N-load cell (type FBB) and 1.5 kN-specimen grips. The dimensions of the rectangular shape test specimen were 60 mm × 15 mm × 0.03 mm (L, l, e) with L the length, l the width and e the thickness as recommended by the standard ISO 14125. Measurements were carried out following an ASTM D638-699 method (1999). Film width was measured using a Traceable® Carbon Fiber Digital Caliper (resolution: 0.1 mm/0.01″; accuracy: ±0.2 mm/0.01″; Fisher Scientific, ON, Canada). UTM parameters were set up for "plastics tensile from position" test type with the following selections: 25 mm effective gauge length, flat specimen shape, 1 number of entries, minimum type. The position rate of machine control was fixed to 1 mm/s. Y- and X-axes were assigned to load (100 N-range) and position (500 mm-range) coordinates respectively. TS (maximum stress, MPa) and TM (modulus, MPa) values were automatically collected after film break due to elongation, using Test Navigator® program.

2.3. Water vapor permeability

Water vapor permeability (WVP) tests were conducted gravimetrically using an ASTM 15.09:E96 method (1983). Films were mechanically sealed onto Vapometer cells (No. 68-1, Twhing-Albert Instrument Co., West Berlin, NJ, USA) containing 30 g of anhydrous calcium chloride (0% RH). The cells were placed in a Shellab 9010L controlled humidity chamber (Sheldon Manufacturing Inc., Cornelius, OR, USA) maintained at 25 °C and 60% RH for 24 h. The amount of water vapor transferred through the film and absorbed by the desiccant was determined from the weight gain of the cell. The assemblies were weighed initially and after 24 h for all samples and up to a maximum of 10% gain. Changes in weight of the cells were recorded to the nearest 10^{-4} g. WVP was calculated according to the combined Fick and Henry laws for gas diffusion through coatings and films, according to the following equation:

$$WVP\,(\mathrm{g\ mm/m^2\,day\,kPa}) = \frac{x\Delta w}{A\Delta P}$$

where x is the film thickness (mm), Δw is the weight gain of the cell (g) after 24 h, A is the area of exposed film ($31.67 \times 10^{-4}\,\mathrm{m^2}$), and ΔP is the differential vapor pressure of water through the film (ΔP = 3.282 kPa at 25 °C).

2.4. Gel swelling property

The test film samples were first dried at 37 °C for 12 h in an incubator and then accurately weighed. The dried films (1 g) were then immersed in distilled water (10 mL) for 1–8 h. The wet weight of the films was measured by taking out the films from the water and blotting with a filter paper to remove the surface adsorbed water followed by immediately weighing the films. The water uptake or swelling property of the films was calculated by the following equation:

$$S = \frac{W_s - W_d}{W_d} \times 100$$

where, S is the percentage of water absorption of the films at equilibrium; W_s and W_d are the weights of the samples in the swollen and dry states, respectively.

2.5. Fourier transform infrared (FTIR) spectroscopy

FTIR spectra of the films were recorded using a Spectrum One spectrophotometer (Perkin–Elmer, Woodbridge, ON, Canada) equipped with an attenuated total reflectance device for solids analysis and a high linearity lithium tantalate detector. Spectra were analyzed using the Spectrum 6.3.5 software. Films were stored at room temperature for 72 h in a desiccator containing saturated NaBr solution to ensure a stabilized atmosphere of 60% RH at 25 °C. Films were then placed onto a zinc selenide crystal, and the analysis was performed within the spectral region of 650–4000 $\mathrm{cm^{-1}}$ with 64 scans recorded at a 4 $\mathrm{cm^{-1}}$ resolution. After attenuation of total reflectance and baseline correction, spectra were normalized with a limit ordinate of 1.5 absorbance units.

2.6. X-ray diffraction

For X-ray diffraction (XRD) analysis, film samples were folded several times to increase the sample thickness. Samples were analyzed between $2\theta = 5^\circ$ and 114° with angle step size $2\theta = 0.02^\circ$ in a D8 Discover X-ray Diffractometer (Bruker AXS Inc., Madison, MI, USA) using a Co Kα (40 kV/35 mA) source.

2.7. Thermo gravimetric analysis (TGA)

Thermo gravimetric analysis of the films was carried out using a TGA 7 (Perkin Elmer, USA) analyzer. Experiments were carried out under nitrogen atmosphere. The weight of the film samples varied from 6 to 8 mg, scanning range was maintained to 50–600 °C and the heating rate was 10 °C/min.

2.8. Differential scanning calorimetric (DSC) analysis

Differential scanning calorimetric analysis was carried out using a Pyris DSC calorimeter (Perkin Elmer). The scanning temperature was from 50 to 220 °C range. The scanning process comprised an initial heating followed by cooling and finally a second temperature scan was performed. The heating/cooling rate was 10 °C/min, under a nitrogen atmosphere.

2.9. Scanning electron microscopy (SEM) analysis

Film samples were prepared for scanning electron microscopy by dropping a 5 mm × 5 mm piece cut from the center of the film into liquid nitrogen and allowing the piece to equilibrate under the liquid nitrogen. The film piece was fractured into several smaller pieces with a prechilled razor blade held in a vice grip. The samples were deposited on an aluminum holder and sputtered with gold–palladium alloy (gold/palladium deposition rate of 30 s equivalent to coating thickness of approximately 50 Å) in a Hummer IV sputter coater. SEM photographs were taken with a Hitachi S-4700 FEG-SEM (Hitachi Canada Ltd., Mississauga, ON, Canada) at a magnification of 40,000×, at room temperature, equipped with an X-ray detector model 7200 (Oxford Instruments, Abingdon, UK) with a resolution at 1.36 eV to 5.9 keV.

2.10. Statistical analysis

To validate the results obtained during different experimental procedure, each analysis was carried out in triplicate in a completely randomized experimental design. An analysis of variance (ANOVA) and multiple comparison tests of Duncan's were used to compare all the results. Differences between means are considered significant when the confidence interval is smaller than 5% ($P \leq 0.05$). The analysis was performed by the PASW Statistics 18 software (IBM Corporation, Somers, NY, USA).

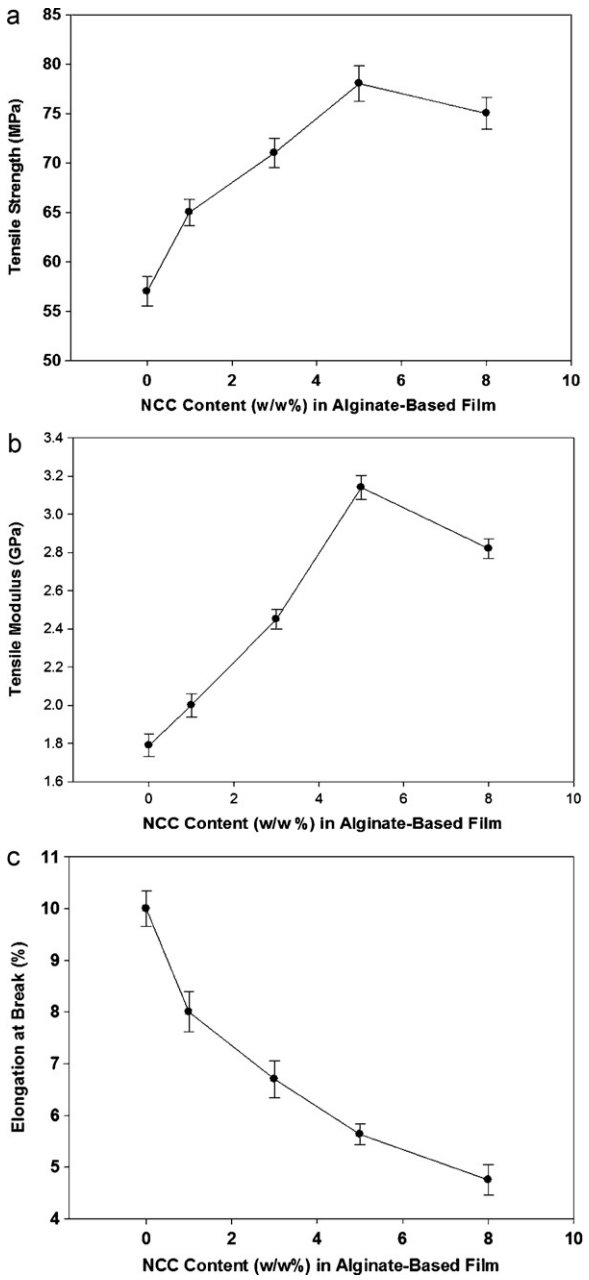

Fig. 1. (a) Effect of NCC content (w/w%) on tensile strength (MPa) of alginate-based film, as a function of NCC content in dry matrix, (b) effect of NCC content (w/w%) on tensile modulus (GPa) of alginate-based film, as a function of NCC content in dry matrix and (c) effect of NCC Content (w/w, %) on elongation at break (%) of alginate-based film, as a function of NCC content in dry matrix.

3. Results and discussion

3.1. Effect of NCC loading on the mechanical properties of alginate-based films

The tensile strength (TS) of pure alginate films was found to be 57 MPa. Fig. 1(a) shows the effect of NCC content on the TS of alginate-based films. Incorporation of NCC caused a significant ($P \leq 0.05$) increase of TS. With 1% NCC, the TS of the films increased to 65 MPa, an increase of 14% compared to the native alginate film. On the other hand, incorporation of 3, 5 and 8% NCC contents raised the TS of alginate-based films by 25, 37 and 32%, respectively. Here NCC acted as a reinforcing agent in alginate-based films and therefore, it imparts higher TS values to the alginate-based films. The improvement of TS attributed due to good interfacial interaction between NCC and alginate-based matrix because of similar polysaccharide structures of cellulose and alginate. It was also observed that the tensile properties of poly (vinyl alcohol)-based composite films were significantly improved with an increase of NCC loading (Lee et al., 2009). Similarly Chang, Jian, Zheng, Yu, and Ma (2010) reported the reinforcing property of NCC with glycerol plasticized starch film.

The tensile modulus (TM) value of the alginate-based films was found to be 1.8 GPa. Fig. 1(b) shows the effect of NCC content on the TM of alginate-based films. Due to the incorporation of 1% NCC into the alginate-based film caused a significant ($P \leq 0.05$) increase of TM to 2.0 GPa, which is an improvement of more than 12% than the native alginate-based films. The highest TM (75% higher than

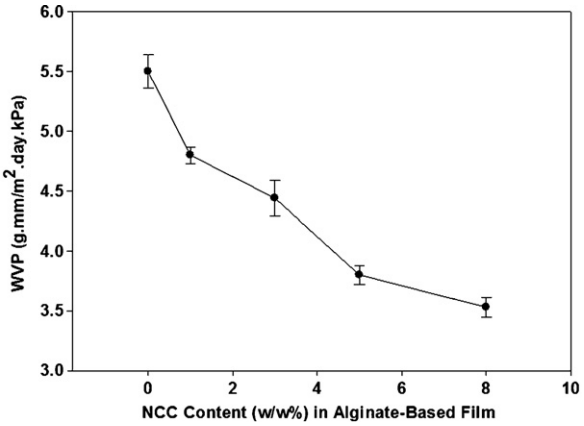

Fig. 2. Effect of NCC content (w/w%) on WVP of alginate-based Film, as a function of NCC content in dry matrix.

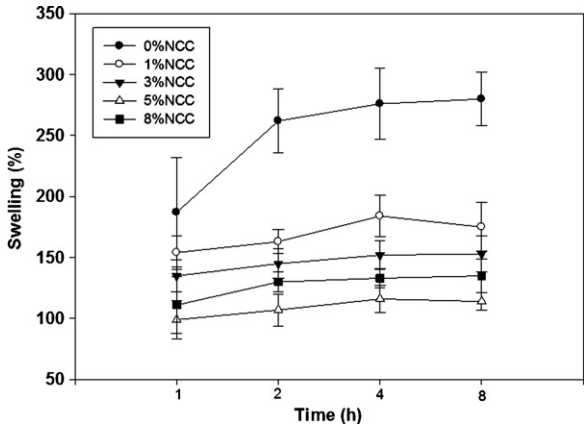

Fig. 3. Effect of NCC Content (w/w%) on swelling of alginate-based film, as a function of NCC content in dry matrix.

that of the control) was observed for 5% NCC loading. All of the NCC-containing specimens showed higher values of TM than the control sample. NCC reinforced biocomposite films became more brittle as the NCC content increases. The increased TM values of the NCC reinforced alginate-based films may be attributed to the increased stiffness of the films by the addition of NCC. Khan et al. (2010a,b) mentioned that the mechanical properties, except elongation, were improved significantly by the addition of cellulose nanocrystals to MC-based films. At low content (5%, w/w), NCC could disperse well in the alginate-based matrix, which increases the mechanical properties (TS and TM) of the nanocomposite. However, high content (8%, w/w) of NCC may be easily agglomerated, which actually could decrease the effective properties of NCC and facilitate to lower the mechanical properties. Fig. 1(c) shows the effect of NCC content on the elongation at break of alginate-based films. The elongation at break (Eb%) values of the alginate-based films were found to be 10%. A significant decrease down to 5% in the Eb value of the alginate-based films was observed for films having a 5% NCC loading, which represents a relative decrease of 44% compared to that of the control sample. Chang et al. (2010) also reported decreased elongations at break with addition of cellulose nanocrystals in plasticized starch-based films.

3.2. Water vapor permeability

Fig. 2 shows the effect of NCC concentration on the WVP of the alginate-based films. The values of WVP decreased with the increase in NCC content. The WVP of control alginate-based films (without NCC) was 5.50 g Mm m^{-2} Day kPa. For all of the alginate-based films loaded with NCC caused lower WVP values compared to those of the control film (i.e. 4.80, 4.44, 3.80 and 3.53 g Mm m^{-2} Day kPa for loadings of 1, 3, 5 and 8% (w/w), respectively). Thus, a significant decrease of more than 31% of WVP was obtained due to only 5% NCC incorporation. Azeredo et al. (2009) reported that the addition of at least 10% (w/w) of cellulose nanocrystals within mango puree-based films was effective to decrease WVP significantly. It was also indicated that after incorporation of 10% (w/w) of cellulose nanocrystals, the WVP of the mango puree-based films was improved 24% compared to the control. The presence of NCC is thought to increase the tortuosity in the alginate-based films leading to slower diffusion processes and hence, to a lower permeability. The barrier properties are enhanced if the filler is less permeable than the matrix and has a good dispersion within the matrix. Sanchez-Garcia, Hilliou, and Lagaron (2010) also demonstrated that after incorporation of 3% (w/w) NCC in carrageenan, the WVP was reduced to 71% compared to the control.

3.3. Gel swelling property

The gel swelling properties of NCC reinforced alginate-based films presents in Fig. 3. Incorporation of NCC significantly reduced the swelling percentage (S) of alginate-based films. After 1 h, the S value of the control alginate films was found to be 187%, whereas due to the incorporation of 5 and 8% NCC, the S values of the composite films were found to be 99% and 111%, respectively. It was also observed that the S values of the NCC reinforced composite films (5%, w/w NCC) decreased about 53% after 8 h of immersion in water than that of the control alginate films. In above experiment, it is reported that WVP of alginate-based films were reduced because of the incorporation of NCC in alginate matrix. So, it was expected to decrease the water uptake of NCC containing alginate films. Ma, Chang, Yang, and Yu (2009) also reported that the addition of low content of nanoparticles in glycerol plasticized starch could result in a dispersion that minimized water absorption.

3.4. Fourier transform infrared spectroscopy

FTIR analysis of films attempted to characterize the incorporation of NCC into alginate-based film matrix by distinguishing the IR bands and vibrations shifts related to NCC-alginate interactions. For native NCC (Fig. 4a), absorption peaks are mainly assignable to O—H stretching vibration at 3600–3200 cm^{-1} (with typical sharpening at 3335 cm^{-1}), symmetric and asymmetric C—H

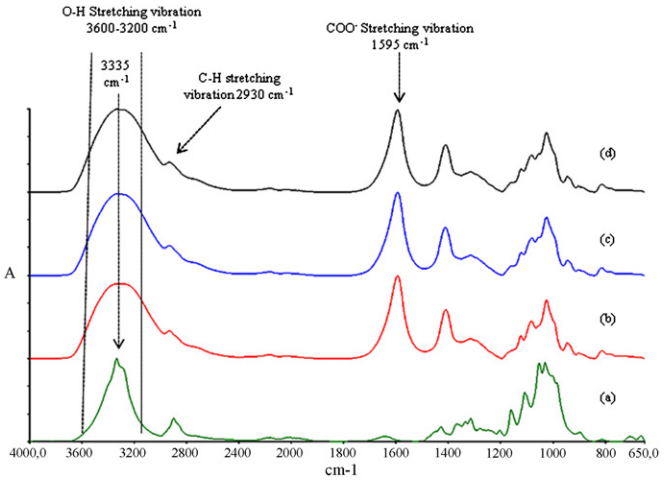

Fig. 4. FTIR spectra of (a) Pure NCC film, (b) native alginate, (c) Alg + 5% (w/w) NCC and (d) Alg + 8% (w/w) NCC.

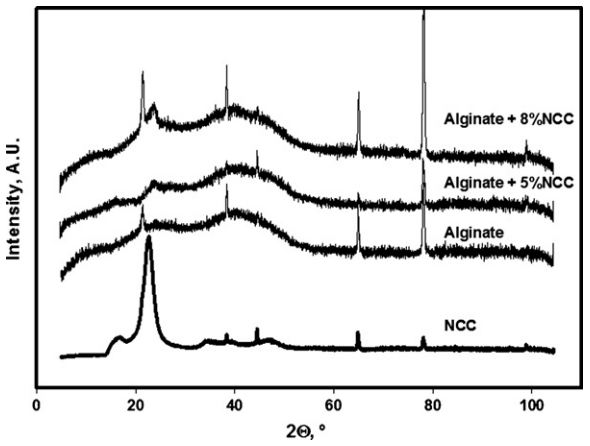

Fig. 5. X-ray diffractograms for NCC, Alginate, Alg + 5% (w/w) NCC and Alg + 8% (w/w) NCC.

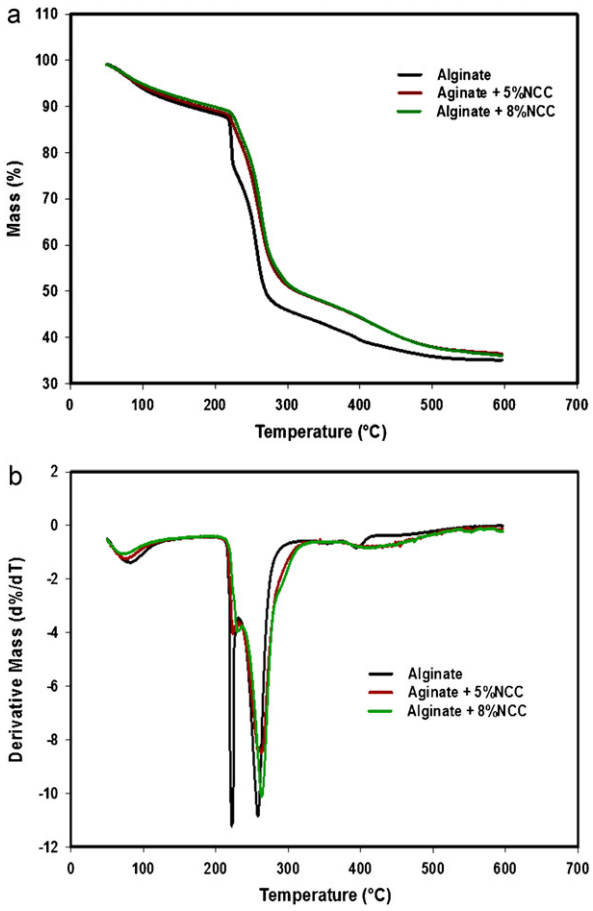

Fig. 6. (a) TGA and (b) derivative TGA curve for Alginate, Alginate + 5% (w/w) NCC and Alginate + 8% (w/w) NCC Film.

stretching vibration of aliphatic chains at 2930 cm^{-1} and bound water vibration at 1645 cm^{-1}, as previously described by Khan et al. (2010a,b). For native alginate film (Fig. 4b), the absorption bands at 3600–3200 cm^{-1} and 1595 cm^{-1} were assigned to the O—H stretching vibrations and to asymmetric and symmetric COO^- stretching vibration, respectively. In addition, peak at 2930 cm^{-1} were ascribed to overlapping symmetric and asymmetric C—H stretching vibration of aliphatic chains (Han et al., 2008). Some differences can be observed after NCC addition into alginate matrix. Indeed, after addition of 5 and 8% NCC (Fig. 4c–d), a slight increase of typical sharpen peak was observed at 3335 cm^{-1} related to O—H vibration of crystalline NCC. Also, the intensity and width of the overall O—H band (3200–3600 cm^{-1}) increased with NCC concentration, suggesting an increase of hydrogen bonding between alginate and NCC (Khan et al., 2010a,b). Moreover, typical sharp band at 3335 cm^{-1} appeared and increased with the addition of NCC content.

Other bands at 1160 and 1055 cm^{-1} had their intensity increased after NCC addition. These bands are attributed to typical cellulosic compounds and are assigned to C—O, C—C and ring structures, in addition to external deformational vibrations of C—H, C—OH, C—CO, and C—CH groups, as already mentioned by Ivanova, Korolenko, Korolik, & Zhbankov (1989). Overall, FTIR spectra of NCC-loaded alginate films provided qualitative insights into the effect of NCC concentration on the position, width and intensity of IR vibrations related to alginate-NCC interactions. Although many bands from alginate spectra masked typical NCC vibrations, especially in the 1800–1270 cm^{-1} fingerprint region (implying bands related to the degree of order of cellulosic materials). FTIR analysis allowed characterizing NCC-alginate molecular interactions via O—H stretching modes (highly related to the degree of hydrogen bonding) and in the 1160–1050 cm^{-1} region, more associated to deformation vibrations of cellulosic compounds.

3.5. X-ray diffraction analysis of the films

XRD analysis was performed in order to analyze the structural property of the alginate and NCC reinforced alginate films. Fig. 5 depicts the diffractograms of NCC, alginate, alginate with 5 and 8% NCC. The diffractogram of alginate consisted of a broad halo (indicator of amorphous nature) containing a sharp peak at around $2\theta = 20^\circ$ indicating crystalline nature. Similar diffractograms for alginate has already reported (Fan et al., 2005; Yang, Zhang, Peng, & Zhong, 2000). In counterpart, the diffractogram of NCC showed the characteristic peaks at $2\theta = 16.8^\circ$ and 20–22.4° (related to more crystalline order) and corresponding to 1 1 0 and 2 0 0 planes of cellulose I, respectively, as already reported by Li, Zhou, & Zhang (2009) and Shin, Gregory, & Exarhos (2007). Incorporation of 5 and 8% NCC into alginate resulted in the presence of an additional peak at $2\theta = 22^\circ$, relatively to the contribution of NCC that allowed increasing the crystallinity of the films. However, the characteristic peak of alginate at $2\theta = 20^\circ$ disappeared for the nanocomposite with 5% NCC content. This could be due to the formation of a percolated nanocomposite structure through proper dispersion of NCC into alginate matrix. In a percolated nanocomposite a proper dispersion of NCC in the polymer matrix may result in the eventual disappearance of any coherent diffraction peak from the matrix. This phenomenon occurs because the nanocomposite does not present ordering. The percolated structure facilitates maximum reinforcement due to large surface area in contact with the matrix, as evident from the mechanical strength of the nanocomposite (Favier & Chanzy, 1995). Also, the intensity of the other peaks at $2\theta = 20^\circ$, 38°, 64° and 77° were reduced at 5% NCC content, possibly due to the effect of resonance generated by percolation. Hence, the main contribution of NCC to induce a higher level of crystallinity was observed in the peak at $2\theta = 22^\circ$ (proportional increase with NCC content). These results are in agreement with all the results observed previously that described improvement of mechanical, barrier and thermal properties as well as chemical interactions between alginate and NCC determined by FTIR analysis.

3.6. Thermal properties of the films

Thermo-gravimetric analysis (TGA) and derivative TGA curves for alginate, alginate with 5 and 8% NCC films are represented

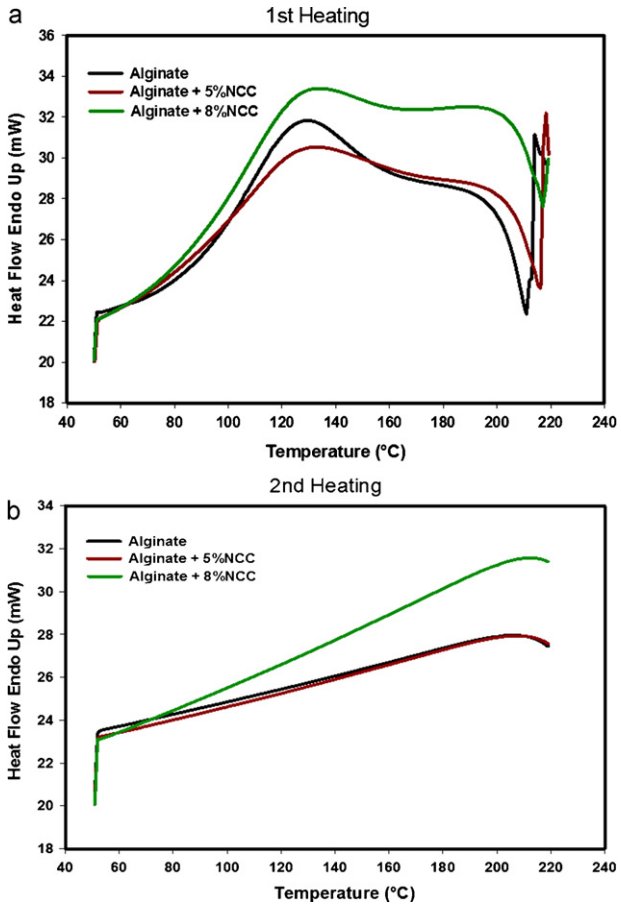

Fig. 7. DSC curves for alginate, alginate with 5 and 8% (w/w) NCC films (a) first heating and (b) second heating.

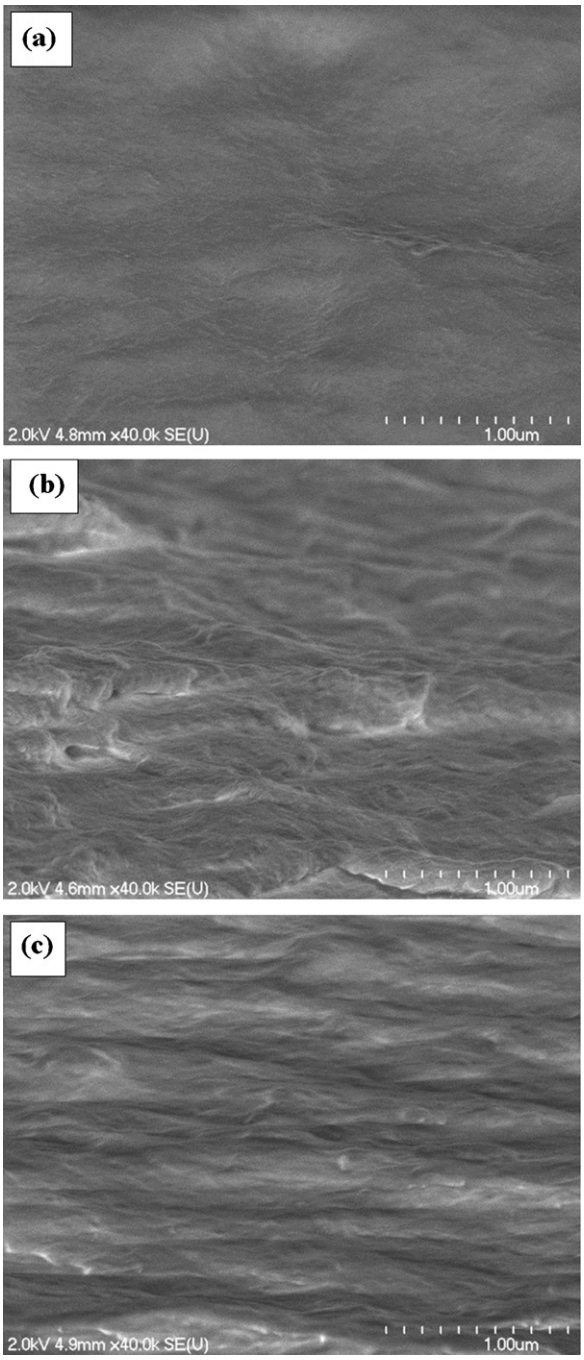

Fig. 8. SEM images of the fracture surface of alginate film (a), alginate film with 5% (w/w) NCC (b) and alginate film with 8% (w/w) NCC (c).

in Fig. 6a and b. The alginate (control) exhibited a decomposition process due to the removal of moisture and surface bound water starting around 206 °C (maximum at 222 °C) with a maximum thermal decomposition occurring at 257 °C. Finally a small change in mass occurred at 388 °C with a total remaining mass accounting for 35% (carbonaceous residues). At 5% NCC, the maximum of the initial decomposition occurred at 223 °C, followed by the second decomposition (maximum at 261 °C). The final carbonaceous content accounted for 36%. At 8% NCC, the maximum of the initial decomposition occurred at 227 °C, followed by the second decomposition (maximum at 263 °C). The final mass accounted for 35%. Hence, the results showed that TGA curves were shifted toward higher temperatures with NCC content, suggesting better thermal stability of NCC reinforced films which also indicated the strong interactions between NCC and alginate matrix. It was also reported that the thermal stability was improved after incorporation of NCC in chitosan based film and glycerol plasticized starch film (Li et al., 2009 and Chang et al., 2010). Derivative curves (Fig. 6b) are in agreement with the results observed for TGA curves and clearly indicated the maximum decomposition phase of the films with a slowing in thermal decomposition with NCC content.

The DSC thermograms of alginate, alginate with 5% NCC and alginate with 8% NCC films are presented in Fig. 7a and b. The first DSC heating cycle shows that all films evolved in similar trends but the heat flow was increased with NCC content (especially at a higher content of NCC). Indeed, a decomposition process was observed from around 210 °C (for control) to 218 °C (for 8% NCC reinforced alginate film). Similar decomposition was observed by TGA analysis. The second DSC heating cycle (Fig. 7b) indicates that the curves did not reveal either crystalline structure or other transition phase. These observations do not point out any thermal decomposition. This is most probably due to the degradation of components during the first heating. Therefore, TGA and DSC curves showed that the addition of NCC in alginate films contributed to a substantial improvement in their thermal stability up to 227 °C.

3.7. Scanning electron microscopy (SEM)

Scanning electron microscopy (SEM) was carried out for extensive morphological inspection of cross-section in NCC reinforced

film. Fig. 8 represents the SEM images of alginate film (a), alginate film with 5% (w/w) NCC (b) and alginate film with 8% (w/w) NCC (c), at 40,000× magnification of the fractured surface (cross-section) of the film. From the SEM image of alginate film (Fig. 8a), it was found that the structure of alginate was composed of interlayer organization, suggesting filamentous (fibrillous) aspect and no susceptible filling as compared to samples containing NCC (5% NCC and 8% NCC). The structure of 5% NCC reinforced alginate film (Fig. 8b) was overall similar to control but interlayers were arranged more closely, with a finer filamentous aspect. Moreover the filling structure looked more compact in presence of NCC. The improved mechanical properties of alginate film with 5% NCC may be attributed to this compact unidirectional interlayer arrangement. Similarly, Azeredo et al. (2009) also reported that the incorporation of NCC in mango puree film showed a compact unidirectional arrangement. For alginate film with 8% NCC (Fig. 8c), the structure was more disorganized (heterogeneous) with the presence of fracture, up and down (serration) shape and less lamellar organization as compared to 5% NCC. These observations could be due to the presence of more NCC aggregates inserted into alginate network and suggesting that NCC has kept much of its original physical properties. Indeed, Chang et al. (2010) reported that higher loading of cellulose nanocrystals did not disperse well in plasticized starch-based films. Overall these SEM observations seem to support all structural modifications and improvements of mechanical and thermal properties related to NCC incorporation in alginate films. Analogous SEM images of NCC into polysaccharide matrices were reported by other studies.

4. Conclusion

It appears that NCC was well dispersed in alginate matrix. So, incorporation of small amount of NCC (5%, w/w) significantly increased the mechanical and barrier properties of the alginate-based matrix. After incorporation of 5% NCC in alginate matrix, tensile and barrier properties were improved compared to the control alginate film. FTIR analysis characterized a molecular interaction between alginate and NCC due to the hydrogen bonding and thermal properties were also improved after incorporation of NCC. Overall, it was optimized that small amount (3–5%, w/w) of NCC had a significant impact on the improvement of physicochemical and thermal properties of alginate-based films.

Acknowledgements

This research was supported by the Natural Sciences and Engineering Research Council of Canada (NSERC) and by FPInnovations (Pointe-Claire, Québec, Canada) through the RDC program. The authors highly appreciated SEM support from Mrs. Line Mongeon, Technician of Biomedical Engineering Department and the Facility Electron Microscopy Research (FEMR) at McGill University. Tanzina Huq is the recipient of a scholarship from Fondation Armand-Frappier.

References

ASTM. (1999). Standard test method for tensile strength of plastics. In *Annual book of ASTM standards*. ASTM International., pp. Method D 638–699.
ASTM. (1983). *Standard test method for water vapor transmission of materials*. Philadelphia, PA: American Society for Testing and Materials. Method 15.09:E96.
Azeredo, H. M. C., Mattoso, L. H. C., Wood, D., Williams, T. G., Bustillos, R. J. A., & McHugh, T. H. (2009). Nanocomposite edible films from mango puree reinforced with cellulose nanofibers. *Journal of Food Science*, *74*(5), 31–35.
Beck-Candanedo, S., Roman, M., & Gray, D. G. (2005). Effect of reaction conditions on the properties and behavior of wood cellulose nanocrystal suspensions. *Biomacromolecules*, *6*, 1048–1054.
Briassoulis, D. (2006). Mechanical performance and design criteria of biodegradable low-tunnel films. *Journal of Polymers and the Environment*, *14*(3), 289–307.
Cha, S. D., Choi, H. J., Chinnan, S. M., & Park, J. H. (2002). Antimicrobial films based on Na-alginate and *k*-carrageenan. *Lebensmittel-Wissenschaft und-Technologie*, *35*, 715–719.
Chang, R. P., Jian, R., Zheng, P., Yu, J., & Ma, X. (2010). Preparation and properties of glycerol plasticized-starch (GPS)/cellulose nanoparticle (CN) composites. *Carbohydrate Polymers*, *79*, 301–305.
Draget, K. I., Braek, G. S., & Smidsrod, O. (1994). Alginic acid gels: The effect of alginate chemical composition and molecular weight. *Carbohydrate Polymers*, *25*, 31–38.
Dong, X. M., Revol, J. F., & Gray, D. G. (1998). Effect of microcrystalline preparation conditions on the formation of colloid crystals of cellulose. *Cellulose*, *5*, 19–32.
Fabra, M. J., Talens, P., & Chiralt, A. (2008). Effect of alginate and λ-carrageenan on tensile properties and water vapor permeability of sodium caseinate-lipid based films. *Carbohydrate Polymers*, *74*(3), 419–426.
Fan, L., Du, Y., Huang, R., Wang, Q., Wang, X., & Zhang, L. (2005). Preparation and characterization of alginate/gelatin blend fibers. *Journal of Applied Polymer Science*, *96*(5), 1625–1629.
Favier, V., & Chanzy, H. (1995). Polymer nanocomposites reinforced by cellulose whiskers. *Macromolecules*, *28*, 6365–6367.
Habibi, Y., Lucia, L. A., & Rojas, O. J. (2010). Cellulose nanocrystals: Chemistry, self-assembly, and applications. *Chemical Reviews*, *110*(6), 3479–3500.
Han, J., Guenier, A. S., Salmieri, S., & Lacroix, M. (2008). Alginate and chitosan functionalization for micronutrient encapsulation. *Journal of Agricultural and Food Chemistry*, *56*, 2528–2535.
Ivanova, N. V., Korolenko, E. A., Korolik, E. V., & Zhbankov, R. G. (1989). IR spectrum of cellulose. *Journal of Applied Spectroscopy*, *51*, 301–306.
Khan, R. A., Salmieri, S., Dussault, D., Calderon, J. U., Kamal, M. R., Safrany, A., et al. (2010). Production and properties of nanocellulose reinforced methylcellulose-based biodegradable films. *Journal of Agricultural and Food Chemistry*, *58*(13), 7878–7885.
Khan, A., Huq, T., Saha, M., Khan, R. A., & Khan, M. A. (2010). Surface modification of calcium alginate fibers with silane and methyl methacrylate monomers. *Journal of Reinforced Plastics and Composites*, *29*(20), 3125–3132.
Klemm, D., Schumann, D., Kramer, F., Koth, D., & Sultanova, B. (2009). Nanocellulose materials: Different cellulose, different functionality. *Macromolecular Symposia*, *280*, 60–71.
Lee, S. Y., Mohan, D. J., Kang, I. A., Doh, G. H., Lee, S., & Han, S. O. (2009). Nanocellulose reinforced PVA composite films: Effects of acid treatment and filler loading. *Fibers and Polymers*, *10*(1), 77–82.
Li, Q., Zhou, J., & Zhang, L. (2009). Structure and properties of the nanocomposite films of chitosan reinforced with cellulose whiskers. *Journal of Polymer Science Part B: Polymer Physics*, *47*, 1069–1077.
Ma, X. F., Chang, P. R., Yang, J. W., & Yu, J. G. (2009). Preparation and properties of glycerol plasticized-pea starch/zinc oxide–starch bionanocomposites. *Carbohydrate Polymers*, *75*, 472–478.
Salmieri, S., & Lacroix, M. (2006). Physicochemical properties of alginate/polycaprolactone-based films containing essential oils. *Journal of Agricultural and Food Chemistry*, *54*, 10205–10214.
Samir, M. A. S. A., Alloin, F., & Dufresne, A. (2005). Review of recent research into cellulosic whiskers, their properties and their application in nanocomposite field. *Biomacromolecules*, *6*, 612–626.
Sanchez-Garcia, M. D., Hilliou, L., & Lagaron, J. M. (2010). Morphology and water barrier properties of nanobiocomposites of k/l-hybrid carrageenan and cellulose nanowhiskers. *Journal of Agricultural and Food Chemistry*, *58*, 12847–12857.
Shin, Y., Gregory, J., & Exarhos, G. J. (2007). Template synthesis of porous titania using cellulose nanocrystals. *Materials Letters*, *61*, 2594–2597.
Yang, G., Zhang, L. N., Peng, T., & Zhong, W. (2000). Effects of Ca^{2+} bridge cross-linking on structure and pervaporation of cellulose/alginate blend membranes. *Journal of Membrane Science*, *175*, 53–60.